New Developments and Challenges in Remote Sensing, Z. Bochenek (ed.)

Fire detection and monitoring by means of MSG: capabilities and restrictions

A. Calle, C. Moclán, J. Sanz & J.L. Casanova
Remote Sensing Laboratory, University of Valladolid, Dp. Applied Physics, Valladolid, Spain

Keywords: MSG-SEVIRI, forest fires detection

ABSTRACT: Detection and parameterization of forest fires is a task traditionally performed by polar-orbiting sensors, mainly AVHRR (A)ATSR, BIRD and MODIS. However, their time resolution is a problem to operate in real time. New geostationary sensors have proven their capacity for Earth observation. GOES, MSG and MTSAT are already operative with time resolutions below 30 minutes. The international community feels that a real-time global observation network may become reality, which is the aim of the Global Observations of Forest Cover and Land Cover Dynamics (GOFC/GOLD) FIRE Mapping and Monitoring program, focusing internationally on decision-taking concerning research into Global Change. This paper shows the operation in real time by the MSG-SEVIRI sensor over the Iberian Peninsula.

1 INTRODUCTION

Despite its limitations the NOAA-AVHRR sensor has been the most important for fire detection and has provided a benchmark for subsequent sensors. An excellent revision of the algorithms used on AVHRR can be found in Li *et al.* (2000). The case of the European sensor Advanced Along Track Scanning Radiometer ((A)ATSR) and the World Fire Atlas from 1997 published by the ESA with the ERS-1 and ERS-2 satellites data (Arino *et al*., 2001) has been used to demonstrate its availability to fire detection (Arino, 2000) and assessment of vegetation fire emissions (Schultz, 2002). The appearance of the MODIS sensor heralded a significant step forward in the observation of forest fires (Kaufman & Justice, 1998; Giglio *et al*., 2003). At this moment, the MODIS fire product is a consolidated product and a reference for global Earth observation (Justice *et al*., 2002). Detection of High Temperature Events (HTE) through geostationary satellites has been taken into account with the different perspective. The improvements introduced in the sensors have allowed us to use geostationary satellites beyond their meteorological capabilities, adapting them to Earth observation. The minimum fire detection sizes of GOES, MSG and MTSAT, with time resolution less than 30 minutes have allowed the international community to think that the global observation network in real time may become reality. The implementation of this network is the aim of the Global Observations of Forest Cover and Land Cover Dynamics (GOFC/GOLD) FIRE Mapping and Monitoring program, internationally focussing on decision-taking concerning research into Global Change. The GOFC/GOLD FIRE program and the Committee on Earth Observation Satellites (CEOS) Land Product validation held a workshop dedicated to the applications of the geostationary

satellites for forest fire monitoring. This workshop was hosted by the European Organization for the Exploitation of Meteorological Satellites (EUMETSAT), whose most relevant conclusions can be seen in Prins *et al*. (2004). The European MSG-1 satellite, the first of the second generation of geostationary satellites operated by the ESA, was launched in August 2002 and is a spin-stabilized satellite. The improvements introduced in the new Meteosat generation have enhanced capabilities for Earth observation (Schmetz *et al*., 2003). This paper shows the capacity of the SEVIRI sensor to perform forest fire monitoring in real time. Some analyses are shown in the particular case of the geographical latitude of the Iberian Peninsula where, during the last two years, detection campaigns and dissemination of results in real time have been carried out.

2 METHODOLOGY

Being a geostationary sensor with a time resolution of 15 minutes, the comparison between successive scenes provides reliable results once the difference temperature threshold is established for such an interval. Thus, if a time thermal gradient, TTG, which is much higher than the one considered normal is detected, we will have a HTE. In order to estimate this gradient let us consider a day's thermal evolution as a sinusoidal curve. According to this model, the maximum difference in the MIR standard temperature between two consecutive SEVIRI scenes is ± 1.5 K for a thermal oscillation of around 30 K, which is typical of summer days in middle latitudes. This estimation agrees with the experimental values found in the analysis of the series of MIR temperature evolution curves selected for different test sites in the Iberian Peninsula during summer. Like this, the maximum temperature difference found, in absolute values, in 98.2% of cases was below 2 K. Only two values above 2.5 K (3.2 and 3.7K) were found, probably due to strong anomalies in the atmospheric conditions since they were very hot days with the presence of vertical turbulent effects. The average differences found, only considering the intervals with thermal variability [05:00–11:00 GMT] and [14:00–20:00 GMT], was 1.2 K, with a standard deviation of 0.5 K. We therefore considered it appropriate to establish a threshold of 4 K as the temperature increase value to detect the outbreak of a fire without incurring in false alarms. We should mention that there are two very well defined daily periods: from sunrise to midday, in which the temperature increases and where the estimation of 4 K is appropriate, and the second between midday and sunset, for which a value of 2–4 K would prove sufficient, being a negative gradient. Detection is easier at night.

In order to estimate the minimum fire size detectable by the SEVIRI sensor, simulations have been performed by means of MODTRAN code by introducing different surface and fire temperatures according to different thermal time gradient values. The radiance observed by sensor was simulated as: $L_{sensor} = p \cdot L_{fire} + (1-p) \cdot L_{surface}$ where p is the surface fraction affected by fire and where two homogeneous phases have been considered; fire and surface. L_{fire} and $L_{surface}$ are the incoming radiances from fire and surface. Spectral radiance was integrated by means of spectral response function and considering different atmospheric attenuation conditions. Results are shown in Figure 1 for a standard atmosphere of middle latitude summer and aerosol depth according to a

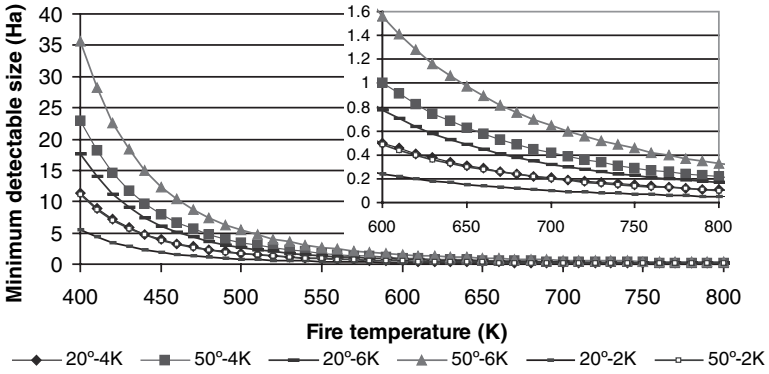

Figure 1. Minimum size of fire (in ha.) to be detected by SEVIRI, for different fire temperature and latitude, taking into account atmospheric attenuation. Three different values of dT/dt are considered: 2 K, 4 K and 6 K.

visibility of 23 km. The abscissa axis shows the potential fire temperature and the ordinate axis shows the minimum detectable area expressed in ha.

Different magnitudes of influence must be analysed separately in Figure 1, the most important being the threshold of TTG considered, dT/dt, but geographic latitude of observation, too. The figure contains the results for three different values of the gradient: 4, 6 and 2 K/15_minutes and for two enclave types at 20° and 50° latitude that define the geographic limits of the occurrence of fire considered in this study. As regards latitude, it must be taken into account that although the pixel area in the nadir point is 9 km^2, at 20° latitude it is 10 km^2 and at 50° it has increased to 18 km^2. Thus, for a required gradient of 4 K/15_min. and a fire of 600 K, the detectable area at 20° latitude is 0.5 ha, whereas at 50° latitude it would be 1ha. The figure shows results for a value of 2 K/15_min that can be applied in the descendant period of daily thermal evolution [14.00–20:00], since during this period $dT/dt < 0$ is expected and the value 2 K/15_min might prove sufficient. This means that during the evening, fires are more easily detected with this method and fire outbreaks can be established at 600 K with 0.24 ha. at 20° latitude and 0.48 ha. at 50° latitude. As can be seen, the detectable sizes during the day at 20° latitude are similar to those in the evening at 50° latitude. These results give a minimum detectable area considerably smaller than presented by Prins & Schmetz, 1999, who did not include atmospheric attenuation. Although comparable, these results are also slightly lower than those presented by Prins *et al*., (2001), who establish 0.2 ha fire detection at 759 K in the Equator and a 0.5 ha fire at 50° latitude. The methodology proposed to detect fire outbreaks is no longer valid as the fire keeps developing since the temperature differences between the different scenes undergo strong variations. Even the frequent appearance of saturated pixels causes sharp changes that cannot be analysed. Further, for the subsequent monitoring of the fire, as will be seen later, a methodology for detecting hot spots is required. Contextual models have been operating on AVHRR and MODIS (Lee and Tag, 199, Kaufman and Justice, 1998, Giglio *et al*., 2003). A contextual analysis, through a spatial matrix of $N \times N$ pixels is carried out on detected fires to verify permanency, establishing the required statistical parameters, averaged value and

standard deviation. According to our results, obtained from the analysis of a data base of fires validated by MODIS, the best window size is N = 9. The detection test ultimately consists of designating an affected pixel as one that fulfils the following:

$$T_{3.9} > \mu_{3.9} + f \cdot \sigma_{3.9}$$

$$T_{3.9} - T_{10.8} > \mu_{dif} + f \cdot \sigma_{dif}$$

where μ and σ are the mean value and the standard deviation in each channel respectively. Although the contextual algorithm has been widely used for other sensors, values have not yet been established for the size of the matrix of analysis applicable to SEVIRI and the statistical factor f. A large interval of values for different sized fires was studied throughout the summer of 2004 and 2005 to obtain detection without the inclusion of a large number of false alarms near the clouds. Finally, our system works with three different values, in the interval $f = [2.9, 3.0, 3.1]$ which show three different levels of probability in the detected fire. Cloud filtering by means of 10.8 μm has been used in order to eliminate low temperature points. It must be said that a contextual detection algorithm applied to MSG images, as applied to images from other polar sensors, would be wholly inadequate to obtain satisfactory results due to the appearance of false alarms. Our aim using contextual analysis was not to present an effective detection algorithm, but rather to present a method to support the detection of HTE once they have started. Our work has shown that this joint process yields good results in the initial detection of HTE and drastically reduces the appearance of false alarms since the contextual process is applied expressly on the points that are already candidates.

Fire monitoring is carried out by means of fire parameterization, such as fire temperature, flaming area and radiative intensity thus being obtained. In order to carry out this analysis, we have applied a technique based on the Dozier methodology (Dozier, 1981; Matson & Dozier, 1981), based on the solving of the following system of equations proposed for bands MIR and TIR. The main restriction when applying Dozier equations is to know the appropriate surface temperature, as small errors imply strong variations in the establishment of the temperature of the fire. We have thus applied the methodology suggested by Giglio & Kendall, 2001, introducing the radiance of the surrounding pixels so that the atmospheric effects and emissivity influence can be taken into account as well as the solar reflective contribution of the small surface in daylight images. In order to know the errors and sensitivity of this methodology, we have simulated fires of different sizes and temperatures, reproducing SEVIRI radiances by means of MODTRAN code through the spectral response functions. Bi-spectral methodology has then been applied on those data in order to establish fire parameters, that is, the reverse process to the previous one. Finally, the comparison between the data calculated from the bi-spectral equations system and the hypothetical simulated fires will give us the errors and sensitivity of this process and its performance in the case of the SEVIRI sensor. Figure 2 shows the results corresponding to an active fire with a pixel fraction of 1e-3 and fire temperature in the interval [450, 1000 K]. The fire-free surface

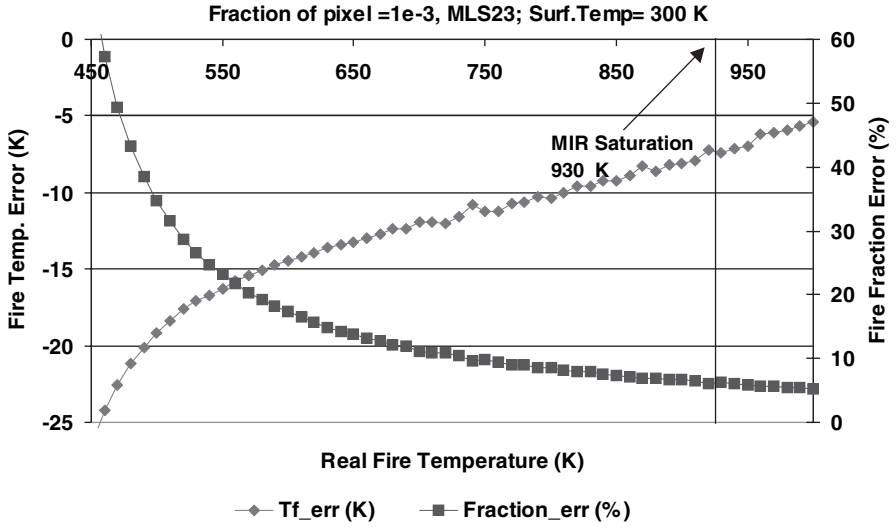

Figure 2. Analysis of errors in determination of fire parameters. The left scale shows the error in the fire temperature and the right scale shows the error in the percentage of fire area. X axis shows real fire temperature.

temperature is 300 K. The figure shows the errors obtained when establishing the parameters of the fire through the establishment of the fire temperature and the flaming area. The first axis of the ordinate shows the difference between the fire temperature, obtained in the reverse process applied to the bi-spectral equations system, and the theoretical fire temperature used in the simulation of the radiance at the sensor's level through the MODTRAN code. As can be seen, the estimated temperature underestimates the real value. Fires with low temperature increase error, that is, whereas at a temperature of 450 K the error is 25 K, at 600 K it is 15 K, and at 900 K there is an error of 8 K. This is a satisfactory result considering this error is way below the one occurring when the atmospheric conditions are unknown. Concerning estimated fire fraction, the percentage error appears in the secondary ordinate axis. According to the results, the pixel fraction affected by fire is the most sensitive magnitude. Hotter fires show smaller errors, as is the case with temperature. We can see stabilization such that from 600 K the error is always below 17%. The figure also shows the zone in which the saturation of the 3.9 μm band would occur, 930 K in the case of a fire with a fraction 1e-3 corresponding to an average of 1.36 ha. at the latitude of the Iberian Peninsula.

3 RESULTS

The summers of 2003–2005 were especially critical in the Iberian Peninsula due to the outbreak of large fires. In the two mid-summer months of 2003 almost 400,000 ha were burned in Portugal. 2005 was catastrophic to the point where fires burned out of control

virtually ‘‘besieging’’ major cities such as Coimbra (Portugal). In Spain, during 2005, nearly 20 people were killed fighting forest fires. One fire alone in the province of Guadalajara (Spain), the most serious of the summer which burned for five days, claimed the lives of 11 people just hours after it started.

Establishing the outbreak of a fire as accurately as possible is crucial to alerting fire-fighting teams as quickly as possible. If the detection process takes into account the comparison with the previous image the delay can be up to 30 minutes in the worst cases. To show some representative results we have analyzed the day on which Spain’s worst fire in the previous decades in terms of human losses occurred. This fire, which started between 12:30 and 12:45 on 16th July 2005, when it was detected by the LATUV, spread for over five consecutive days and devastated around 13,000 ha. Figure 3 shows the image of the 3.9 μm band corresponding to a few hours after the fire. The visual analysis of the image shows the existence of many fires in Spain and Portugal. Given their importance, two have been highlighted and shown. Number 1 is the fire in Guadalajara (Spain) that claimed the lives of 11 people and number 2, one of the fires that affected the natural park of Lago de Sanabria (Zamora, Spain) during the summer of 2005, whose initial

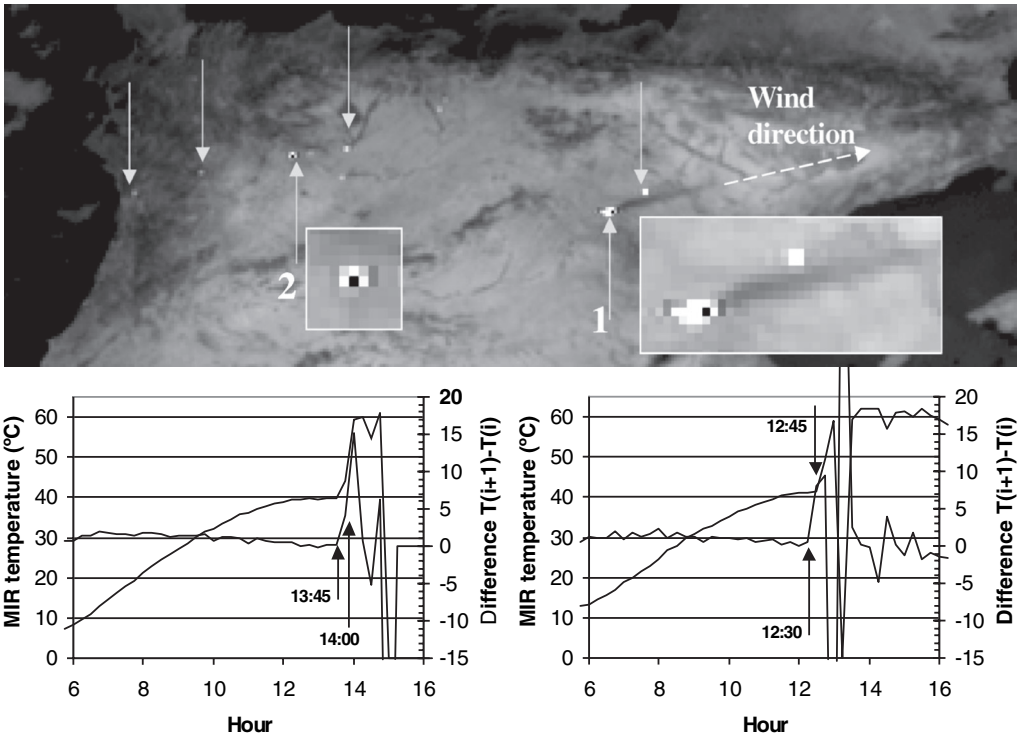

Figure 3. This figure shows the methodology to detect the start of a fire. The upper part is the 3.9 μm band, highlighting several fires (validated by MODIS). The second part shows the thermal evolution, in the left scale, and the time thermal gradient, in the right scale, in °C/15_minutes, for the two selected cases #1 and #2.

characteristics, as will be seen, differ from the first. In the figure, we have indicated the wind direction in fire #1 from the smoke plume, which is perfectly visible and which will be useful later to analyze the spread of the fire. Below in the same figure are the two thermal evolution diagrams corresponding to these fires. The diagram shows the temperature evolution of band 3.9 μm, in °C, in the primary axis of the ordinate according to the time of the day, between 06:00 and 16:00 GMT. The secondary axis of the ordinate shows the evolution of the time thermal gradient of the same band, in °C/15_minutes. If we compare both temperature evolution curves, we can see that they are practically identical on the primary axis up to the moment at which the fire starts, at 12:30 in #1 and at 13:45 in #2 despite being different vegetation covers with different fuel moisture content since they occur in different climate zones. The analysis of the curve of the time thermal gradient is much more conclusive. The change in the temperature value is 1.5°C/15_minutes in both curves prior to the outbreak of the fire reaching a maximum of 2.3 in #1 and 1.8 in #2, which are exceptional considering the rest of the values. Standard deviation was approximately 0.5 in both cases. These results are coherent with the theoretical analysis in the previous paragraph. Case #2 was a fire that started with a time thermal gradient of 4.2°C/15_minutes in the first scene at 14:00 GMT, immediately jumping to 15°C/15_minutes in the following scene at 14:15 GMT. It is clear that it began between 13:45 and 14:00 as the figure shows. The case of fire #1 presents a much more abrupt beginning, with a time thermal gradient of 8°C/15_minutes in the first scene at 12.45 GMT. In this case, the fire broke out between 12:30 and 12:45 GMT. These results entirely agree with the comments in the methodology paragraph, where the value 4°C/15_minutes was presented as the initial detection threshold. Apart from its initial causes, the characteristics of a fire at its onset depend on the combustible material and moisture. In this comparison, it is not surprising that the outbreak was slower in case #2, whose gradient was below #1, as this was a climate zone with higher moisture content. Other fires have been analyzed and the same qualitative characteristics have been found.

Figure 4 shows the results corresponding to the operating capacity of real-time fire detection, where we can see the most recent observations corresponding to the last period, August-November 2005. Figure 4 shows the map of fires detected in the three countries in the Mediterranean area analysed: Spain, Portugal and the South of France. As can be seen, the most affected areas were located, very critically, in the northern half of Portugal, a country where a total of 517 fires were detected during that period of time. The Northwest of Spain was greatly affected by fires, with a total of 487 fires in this region. The fires in France were concentrated around the Gulf of Leon area, although with a much smaller occurrence of fires than in the previous cases, with a total of 24 fires.

4 RESTRICTIONS

As regards sensor restrictions, the most important problem is saturation. The operative range of the SEVIRI sensor reaches up to 335 K. This value is similar to the AVHRR (Robinson, 1991) and even higher than (A)ATSR with 312 K, which has also been used for fire detection (Arino, 2000) although below MODIS (Kaufman & Justice, 1998) and of course, less than other sensors with a higher spatial thermal resolution such as BIRD (Lorentz & Skrbek, 2001). This might seem high enough to observe any type of fire and

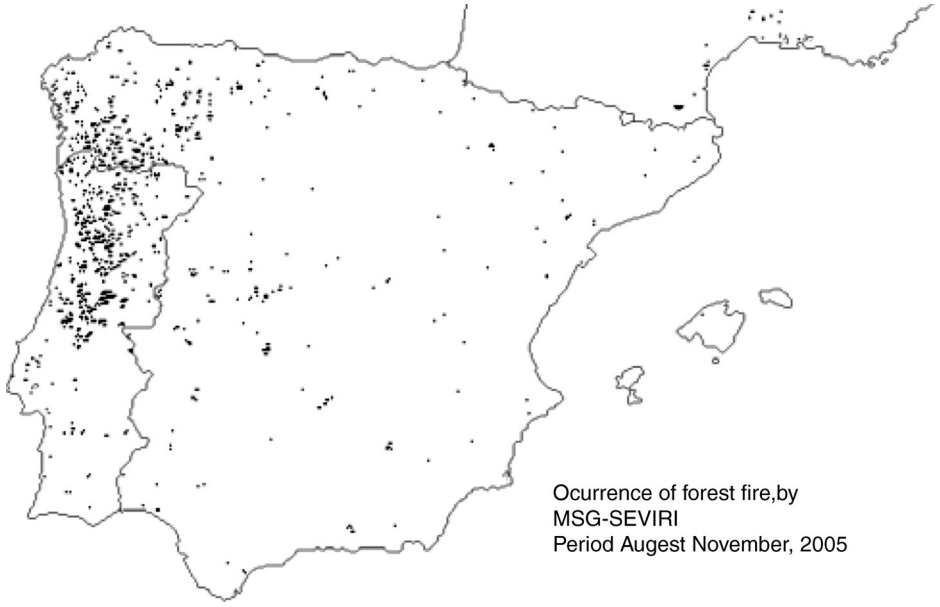

Figure 4. Map of fire occurrence in Spain, Portugal and Southern France corresponding to August-November, 2005.

establish its parameters since the SEVIRI pixel area is an order of magnitude greater than the ones mentioned. However, the 3.9 μm band [3.48–4.36 μm] appears saturated relatively frequently in several types of fires observed. This situation has advantages since saturation ensures detection without the possibility of false alarms. However, the radiometric information and the possibility of obtaining fire parameters have been lost.

For a geostationary sensor, analysis of the factors that cause the sensor's saturation involves considering the latitude, given the variability of the area of each pixel. In order to establish the saturation conditions, we simulated the radiance that the SEVIRI sensor receives for different fire temperatures and different affected areas by limiting these conditions for an apparent temperature value of 335 K. Figure 5 shows the fire area expressed in ha that would cause the sensor's saturation according to the fire temperature. The figure shows different geographical locations at 20°, 30°, 40° and 50°. The atmospheric conditions correspond to a standard profile of the mid-summer latitudes with 23 km visibility. Thus, a typical fire with a temperature of 600 K observed at 50° latitude would lead to saturation with an active area close to 18.5 ha. If the observation had been carried out at 20° latitude, half of that surface would have been enough for saturation. The atmospheric conditions have a certain influence over these results. Thus, considering a strong concentration of aerosols that reduce visibility at 5 km, the fire area that causes the saturation must be increased in a percentage whose value is independent of its temperature. However, this percentage increases with the latitude. Thus, the surfaces that cause saturation when going from 23 km to 5 km visibility for the latitudes of 20°, 30°, 40° and 50° increase respectively by 10%, 12%, 14% and 18%.

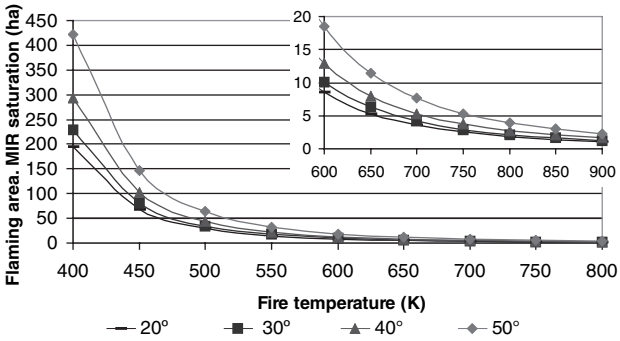

Figure 5. FIRE flaming area, in hectares, that leads to saturation on the 3.9 μm band, versus fire temperature. The graph shows these results for different geographic latitudes, 20°, 30°, 40° and 50°, taking into account atmospheric effects.

Other important restriction of the SEVIRI sensor is the sampling method. Spatial resolution of SEVIRI is 4.8 km at nadir, with a oversampling of 1.6 km. Step of sampling of pixels is 3 km; so radiance obtained in each pixel is coming from more than 3 km and even, there is common radiance between neighbour pixels. The MSG observations of active fires in the 3.9 μm channel exhibit and distinct star or ''plus sign'' pattern in the x, y directions because of over-sampling. In estimating the subpixel characteristics we have used the center pixel in their calculations. Figure 6 shows this restriction for different patterns of fires detected.

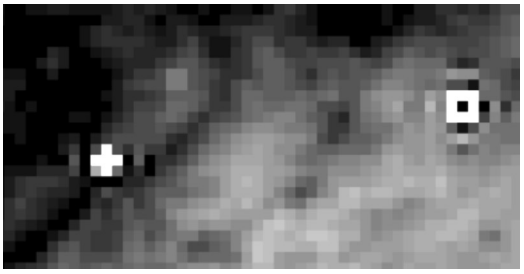

Figure 6. Pattern of sampling of pixels affected by fire.

5 CONCLUSION

In the light of the results, the SEVIRI geostationary sensor proves to be a highly efficient tool in real-time forest fire management and monitoring. Despite not being originally designed as an Earth observation tool, but as a meteorological satellite, its excellent time resolution of 15 minutes has proved useful for the detection of events which vary due to

radiometric rather than spatial characteristics, as is the case of forest fires. Detection based on the 3.9 μm band is possible, although its spatial resolution does not make it possible to locate the event accurately enough to provide early waning useful for fire fighting tasks. Minimum size detected can be 0.7 ha in a fire of 600 K in the Iberian Peninsula. With regard to the methodology for obtaining parameters, it can be transferred from other sensors, such as MODIS, although fire sizes have to be taken into account. The experimental methodology can be applied under very specific conditions. It has been proved that a geostationary system with a very simple configuration and observation geometry might be the long sought after real-time global fire control system. For this purpose, further research into higher spatial resolution thermal sensors needs to be performed.

ACKNOWLEDGMENTS

This paper has been carried out within the Project entitled: ''Estudio y seguimiento de los incendios forestales en Castilla y León, en tiempo real, mediante técnicas de teledetección espacial'', ref. VA017A05 founded by Junta de Castilla y León. The authors wish to thank the Institution that has made this paper possible.

REFERENCES

Arino, O. and Mellinote, J.M. (1998), The 1993 Africa fire map, *Int. J. Remote Sensing*, 19, 2019–2023.

Arino, O., Paganini, M., Simon, M., Ferruchi, F., Barro, E., Benvenuti, M., Chuvieco, E., Dwyer, E. and Fierens, F. (2001), Current and future activities of ESA related to forest fires, *Proceedings of the EARSeL 3rd Iinternational Workshop*, Paris, 17–18 May 2001.

Arino (2000). Various Authors. ATSR World Fire Atlas validation. *ESA-ESRIN, Italy.*

Berk, A., Bernstein, L. W. and Robertson, D.C. (1996), MODTRAN: A moderate resolution model for LOWTRAN 7, *Philips Laboratory, Report* AFGL-TR-83-0187, Hanscom ARB, MA. 1983.

Briess, K., Jahn, H., Lorenz, E., Oertel, D., Skrbek, W. and Zhukov, B. (2003), Fire recognition potential of the bi-spectral detection (BIRD) satellite, *Int. J. Remote Sensing*, 24, 865–872.

Calle, A., Casanova, J. L., Moclán, C., Sanz, J., Goldammer, J, Li ZengYuan and Qin Xianlin, (2005), DRAGON Symposium organized by ESA and NRSCC of China. Santorini (Greece), June 2005.

Dozier, J. (1981), A method for satellite identification of surface temperature fields of subpixel resolution, *Rem. Sens. of Env.*, 11, 221–229.

Giglio, L and Kendall, J.D., (2001), Application of the Dozier retrieval to wildfire characterization. A sensitivity analysis, *Rem. Sens. of Env.*, 77, 34–49.

Giglio, L. and Justice, C.O., (2003), Effect of wavelength selection on characterization of fire size and temperature, *Int. J. Remote Sensing*, 24, 3515–3520.

Ichoku, C., Kaufman, Y.J., Giglio, L., Li, Z., Fraser, R.H., Jin, J-Z and Park, W.M. (2003), Comparative analysis of daytime fire detection algorithms using AVHRR data for the 1995 fire season in Canada: perspective for MODIS, *Int. J. Remote Sensing*, 24, 1669–1690.

Justice, C.O., Giglio, L., Korontzi, S., Owens, J., Morisette, J.T., Roy, D., Descloitres, J., Alleaume, S., Peticolin, F. and Kaufman, Y. (2002), The MODIS Fires Products, *Rem. Sens. of Env.*, 83, 244–262.

Justice, C.O. and Korontzi, S. (2001), A review of satellite fire monitoring and requirements for global environmental change research, *In Global and Regional Wildfire Monitoring: Current status and future plans (F.J. Ahern, J.G. Goldammer, C.O. Justice, Eds.)*, SPB Academic Publishing, The Hague, Netherlands, pp. 1–18.

Kaufman, Y. and Justice, C. (1998), MODIS Fire Products, Algorithm Theoretical Basis Document. MODIS Science Team. EOS ID#2741.

Li, Z., Kaufman, Y.K., Ichoku, C., Fraser, R., Trishchenko, A., Giglio, L., Jin, J. and Yu, X. (1999). A review of AVHRR-based active fire detection algorithms: Principles, limitations and recommendations. *Forest Fire Monitoring and Mapping: A Component of Global Observation of Forest Cover, Editors: Ahern, Gregoire and Justice*, Ispra, Italy, 3–5 November 1999.

Lorentz, E. and Skrbek, W. (2001), Calibration of a bi-spectral infrared push-broom imager. *Proceedings of SPIE, Infrared Spaceborne Remote Sensing IX*, San Diego, 29 july-3 August 2001.

Langaas, S. (1995). A critical review of sub-resolution fire detection techniques and principles using thermal satellite data. *Ph.D. thesis. Department of Geography.* University of Oslo. Norway.

Matson, M. and Dozier, J. (1981), Identification of sub-resolution high temperatures sources using a thermal IR sensor. *Photo Engr. and Remote Sensing*, 47(9), 1311–1318.

Prins, E.M. and Menzel, W.P. (1992), Geostationary satellite detection of biomass burning in South America, *Int. J. Remote Sensing*, 13, 2783–2799.

Prins, E.M. and Menzel, W.P. (1994), Trends in South American burning detected with the GOES VAS from 1983–1991. *J. Geophys. Res.*, 99(D8), 16719–16735.

Prins, E and Schmetz, J. (1999), Diurnal fire active detection using a suite of international geostationary satellites. *GOFC Forest Fire Monitoring and Mapping Workshop*, JRC, Ispra.

Prins, E., Schmetz, J., Flynn, L., Hillger, D. and Fetz, J. (2001), Overview of current and future diurnal active fire monitoring using a suite of international geostationary satellites. *Global and Regional wildfire monitoring: current status and future plans, F. J. Ahern, J. G. Goldammer and C. O. Justice Eds.*, SPB Academic publishing, 145–170.

Robinson, J.M., (1991), Fire from space: Global fire evaluation using infrared remote sensing. *Int. J. of Remote Sensing*, 12, pp. 3–24.

Schmetz, J., Pili, P., Tjemkes, S., Just, D., Kerkmann, J, Rota, S., & Ratier, A. (2002) An Introduction to Meteosat Second Generation (MSG), BAMS, 83, 977–992.

Schmetz, J., Konig, M., Pili, P., Rota, S., Ratier, A. and Tjemkes, S. (2003), Meteosat Second Generation (MSG): Status after launch. *Preprints, 12th conference on Satellite Meteorology and Oceanography*, Long Beach, C.A., Amer.Meteor. Soc., CD-ROM. P7.3.

Schultz, M. (2002), On the use of ATSR fire count data to estimate the seasonal and inter-annual variability of vegetation fire emissions. *Atmosph. Chem. and Phys.*, 2, 387–395, 2002.